

Electronic and Thermoelectric Properties on Rutile SnO₂ Under Compressive and Tensile Strains Engineering

Budi Adiperdana^{a,*}, Nadya Larasati Kartika^b, Irwan Ary Dharmawan^c

^aDepartement of Physics
Universitas Padjadjaran
Jl. Ir. Soekarno km.21
Sumedang, Indonesia

^bResearch Center for Advanced Materials
National Research and Innovation Agency
Komplek BRIN Jl. Sangkuriang No. 21
Bandung, Indonesia

^cDepartement of Geophysics
Universitas Padjadjaran
Jl. Ir. Soekarno km.21
Sumedang, Indonesia

Abstract

SnO₂ has the potential to be an environmentally friendly thermoelectric material. To obtain the optimum properties of this material, strain engineering is used to investigate the electronic and thermoelectric properties. In this study, we used compressive and tensile strains with -5%, -2%, 0%, 2%, 5%, and 10% in three schemes; they are triaxial (ϵ_{abc}), biaxial (ϵ_{ab}), and uniaxial (ϵ_c) strains. All model structures are calculated based on density functional theory (DFT) with several exchange-correlation functionals. The presented results show that strain engineering enhances the Seebeck coefficient for a compressive strain parameter since the energy gap between the conduction and valence band increased due to the strong covalent bonding at the conduction band. From several comparisons in bandgap and thermoelectric properties calculation between PBEsol and PBE0, this study suggests that PBE0 is effectively used to calculate the energy gap. Meanwhile, for thermoelectric properties, PBEsol gave the best-estimated value. In addition, this study explained that the largest or the smallest bandgap could be achieved by varying strain simply on the *c*-axis as the optimum manipulation of the SnO₂ structure. Furthermore, this paper also revealed that the simulation strategy could be determined from the desired result, whether to enhance the Seebeck coefficient or the electrical conductivity by manipulating the *ab*-axis and the *c*-axis, respectively.

Keywords: strain, DFT, exchange-correlation, thermoelectric, bandgap.

I. INTRODUCTION

Tin dioxide (SnO₂) is a wide-bandgap oxide material with an n-type semiconductor. SnO₂ can be grown as a tetragonal rutile structure ($P4_2/nmn$), the most commonly available and stable among other structure types [1]. The properties of this material have led to being applied in several useful devices since tin dioxides exhibit a 3.6 eV bandgap [1]-[2], high conductivity, and optical transparency in the visible region [3]. By tuning the properties, SnO₂ shows significant potential in the application of transparent conductors [4] and gas sensing technology [1], and recently SnO₂ has been showing the possibility of being an environmentally friendly thermoelectric material due to its stability in high temperature [5].

Thermoelectric materials play an important role in determining efficiency and are quantified by the dimensionless figure of merit (ZT) [6]-[7],

$$ZT = \frac{S^2 \sigma T}{\kappa} = \frac{PF}{\kappa} \quad (1)$$

where S is the Seebeck coefficient which represents a significant ratio between the temperature gradient and generates electricity which is defined by $S = \Delta V / \Delta T$, σ is the electrical conductivity, T is an absolute temperature, PF is the power factor, and κ is the total thermal conductivity obtained from the lattice thermal conductivity (κ_L) and the electronic thermal conductivity (κ_e). To improve the ZT , based on (1), the thermoelectric materials should have high electrical conductivity and low thermal conductivity at the same time. Besides being a parent material, tin dioxide is used as a composite for other primary structure materials. Nugraha *et al.* did for Bi₂Te₃ as the main structure of the composite materials [8]. However, the large thermal conductivity in SnO₂ still limits the performance of the thermopower with a value of around 40 Wm⁻¹K⁻¹ [9].

Several strategies have been carried out to overcome the limitation of the SnO₂ materials. Bagheri *et al.* improved the Seebeck coefficient from -255 μ V/K to *p*-type 1850 μ V/K at 350 K by doped SnO₂ with 7.8% iron [10]. The enhancement of power factor and figure of merit obtained by doping SnO₂ with Sb was studied by Rubenis *et al.* [11]. Moreover, nanostructuring was also

* Corresponding Author.

Email: b.adiperdana@unpad.ac.id

Received: October 12, 2022 ; Revised: December 15, 2022

Accepted: December 19, 2022 ; Published: December 31, 2022

applied to improve the SnO₂ performance; Kartika *et al.* and Delorme *et al.* could increase the Seebeck coefficient and lower thermal conductivity, respectively [12]-[13].

The different synthesis process, which involves various parameters in SnO₂, or other oxide materials, often results in the appearance of strains in the lattice parameter due to the changes in the crystal structure [14]. Moreover, since the band structure of semiconductors can be varied by the interatomic distances and atomic positions, it is commonly recognized that strain can affect the electronic structure of semiconductors [15] and improve their thermoelectric performances. Some works that applied strain parameters in their study are Absike *et al.* [16], who studied copper oxide and obtained enhancement in the Seebeck coefficient and carrier concentration. Meanwhile, through computation calculation, Kerrami *et al.* [5] showed improvement of the figure of merit of tin dioxide at high temperatures under strain towards *a* and *b* varied lattice constant.

Computation modelling material is a reliable tool to examine the strain effect on the bandgap and the thermoelectric properties of tin dioxide through theoretical approximation. This work aims to characterize the structural, electronic, and thermoelectric properties of SnO₂ using the density functional theory (DFT) [17]. The DFT is a low-cost, time-saving quantum mechanical theory to compute many physical characteristics of solids with high precision. In the DFT, the Schrödinger equation for many body systems is simplified to the Kohn-Sham equation [17], a single particle-independent Schrödinger equation that can be easily numerically solved. One of the keys to achieving chemical accuracy in the DFT is to expand the exchange correlation based on higher-density functional derivative, $E_{xc}[\rho, \nabla\rho, \nabla^2\rho]$. Therefore, it is crucial to obtain a near-accurate bandgap value; hence, several types of exchange-correlation parameters are used in this paper. They are generalized gradient approximation (GGA), meta-GGA, and hybrid exchange-correlation functional.

The GGA exchange correlation is used in the form of the PBEsol functional, a modified version of the GGA Perdew-Burke-Ernzerhof (PBE) functional that is used specifically to generate lattice constants for solids [18]. The Gau-PBE or Gaussian attenuation PBE is the function used from the meta-GGA, this type of exchange-correlation functional bridges between the expensive calculation in hybrid functional with simple GGA calculations by using a Gaussian attenuation scheme (Gau) to include a short-range Hartree-Fock (HF) exchange [19]. Increasing the exchange-correlation terms can attain better chemical accuracy. Therefore, the hybrid functional is employed in the thermoelectric properties' calculation. The exchange correlation from the hybrid form is PBE0 [20] and Heyd-Scuseria-Ernzerhof (HSE) [21]. PBE0 and HSE functionals involve the exact exchange calculation as an energy correction to ensure that the energy level is as close as possible to the experiment result. The difference between PBE0 and HSE lies in the hybrid ratio between the DFT and other approximations. PBE0 functional combines the PBE exchange energy and Hartree-Fock (HF) exchange energy in a ratio of 3:1 [20]; in contrast, the HSE exchange-correlation function calculates the exchange

part of the energy using an error-function-screened Coulomb potential to improve computational efficiency [21].

The highlight of this paper is to give strain variations towards the *a*, *b*, and *c* axis simultaneously (ϵ_{abc}), biaxial strain towards the *a* and *b* axis (ϵ_{ab}), and uniaxial strain towards the *c*-axis (ϵ_c), since the studies of strain effect in SnO₂ are still limited, especially in the thermoelectric properties, it is quite thought-provoking to be discussed through theoretical approximation to shed some light on this area.

II. METHODS

The calculation was implemented using the Quantum ESPRESSO 7.0 [22] using the density functional theory (DFT) with projector augmented wave (PAW) pseudopotentials [23] to perform a self-consistent field (SCF) calculation. The energy cut-off is set to be 4.23669×10^2 Ry for the SCF calculation. In this study, all computations were performed using the SnO₂ unit cell in a rutile crystal structure. The computational model of this study is shown in Figure 1, which represents the normal structure and strain directions. The positive and negative strains were applied using three schemes; they are strain in *abc*-axis direction (ϵ_{abc}) for triaxial strain, *ab*-axis (ϵ_{ab}) for biaxial strain, and *c*-axis alone (ϵ_c) for uniaxial strain. Then the optimum applied strain scheme was investigated to increase the bandgap and the thermoelectric properties. Strain variations for each scheme are -5%, -2%, 0%, 2%, 5%, and 10%. The detail of the model simulation is summarized in Table 1, where strain variation was applied for positive and negative treatment, representing tensile and compressive strain, respectively.

All the unstrained and strained unit cell relaxation structures were performed in Perdew-Burke-Ernzerhof revised for solids (PBEsol) as an exchange-correlation (XC) parameter. Then, the band structure calculation was performed in WANNIER90 [24] using the generalized gradient approximation (GGA), the meta-GGA, and the

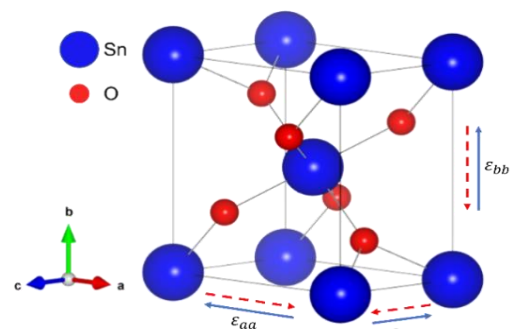


Figure 1. Ball and stick model on SnO₂ simulation with strain variations.

TABLE 1
A COMPUTATIONAL MODEL FOR TIN DIOXIDE SIMULATION

Structure volume	Model
100%	Stable structure
95%	5% negative strain
98%	2% negative strain
102%	2% positive strain
105%	5% positive strain
110%	10% positive strain

hybrid functional with both k-point and q-point of $2 \times 2 \times 2$. As mentioned before, four types of XC were used to find the best approximation for the SnO_2 system: the generalized gradient approximation (GGA) PBESol, the meta-GGA Gaussian attenuation PBE (Gau-PBE), PBE0, and Heyd-Scuseria-Ernzerhof (HSE) as the form of the hybrid exchange functional. These preliminary operations were used to ensure that the method for bandgap approximation in this work was as close as to the experiment result, which was somewhere around 3.4–4.0 eV [1], [5].

After studying the basic structural stability and electronic properties of bulk SnO_2 , the Seebeck thermoelectric properties and electronic conductivity were obtained by solving the semi-classical Boltzmann equation transport, which was investigated using BOLTZWANN [25]. The thermoelectric properties calculation was carried out in a temperature range of 100 to 800 K according to several experimental results that have been done previously.

III. RESULTS AND DISCUSSIONS

A. Bandgap Calculation

Band structure calculation using PBESol, gau-PBE, PBE0, and HSE exchange-correlation parameters are shown in Figure 2(a) - 2(d), respectively, and the bandgap values for each graph are shown in Table 2. As is observed, the minimum energy gap occurs in the Γ and M directions, and the bandgap value derived from the four exchange-correlation factors discussed above clearly differs from one another. The PBESol parameter gives the widest bandgap with a 2.99 eV discrepancy ($E_{gap}^{xc} - E_{gap}^{Exp}$) compared with the experimental value [5]. Meanwhile, the narrowest bandgap is shown by the PBE0 hybrid functional, and it is set as an optimum exchange-correlation parameter for bandgap calculation in SnO_2

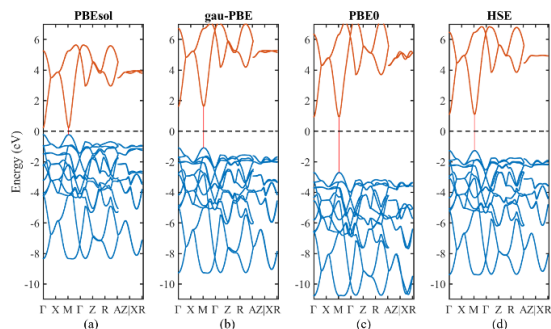


Figure 2. Band structure of SnO_2 using several exchange-correlation parameters: (a) PBESol; (b) gau-PBE; (c) PBE0; and (d) HSE.

TABLE 2
THE BANDGAP FOR EACH EXCHANGE-CORRELATION WITH THE DIFFERENCE IN THE EXPERIMENT

Exchange-correlation type	E_{gap} (eV)	$ E_{gap}^{xc} - E_{gap}^{Exp} $ (eV)
Exp. [5]	3.6	-
GGA-PBESol	0.6025	2.9975
Meta-GGA gau-PBE	2.7242	0.8758
Hybrid PBE0	3.1440	0.4560
Hybrid HSE	2.3829	1.2171

with a 0.45 eV difference from the experimental result. A previous paper [26] assessing the structural calculation on transparent conducting oxide also used PBE0 functional for SnO_2 DFT calculation. Moreover, the calculation using PBE0 approximation has proven that the structural and bandgap data are in excellent agreement with experimental value and much improved from other hybrid exchange functionals that have been examined on SnO_2 , such as HSE06 [27]-[28].

The default electron-exchange hybrid value for PBE0 is 25% in Quantum ESPRESSO, which needs to be investigated to achieve a better bandgap. The hybrid value is set with 5%, 25%, 50%, 75%, and 95% of exchange parameters. The result shown in Figure 3(a) depicts the linearity between the gap energy and the hybrid exchange factor, where the conduction band minimum (CBM) and valence band maximum (VBM) have different linearity tendencies. The Fermi energy, however, clearly stays closer to the conduction band than the VBM despite the change in the exchange parameter percentage value, indicating an n-type semiconductor. In order to determine the best hybrid exchange percentage, linear interpolation was used, and the results show that 29% is the best approximation towards the experimental value, as shown in Figure 3(b).

The unit cell structure of tin dioxide with several types of strain effect was carried out by including the atomic relaxation to make the calculation result nearly possible. The structure could only be relaxed by PBESol due to the low cost of the calculation. Then the strain effects on the bandgap structure process were calculated using PBESol for the relaxation process and PBE0 to generate the energy gap. In addition, bandgap calculations were also performed using PBESol for comparison.

The effect of the uniaxial (ϵ_c), biaxial (ϵ_{ab}), and triaxial strain (ϵ_{abc}) on the lattice parameter are shown in Figure 4(a) for a and b lattice parameters and Figure 4(b)

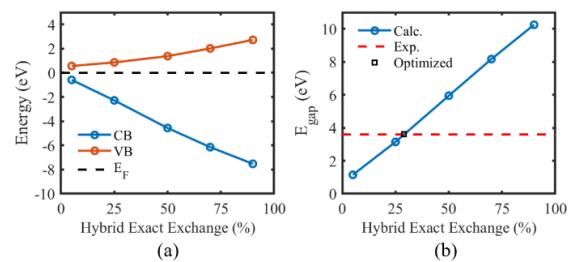


Figure 3. Effect of hybrid exact exchange percent to (a) valence band maximum, conduction band minimum and Fermi level; (b) energy gap compared to experiment.

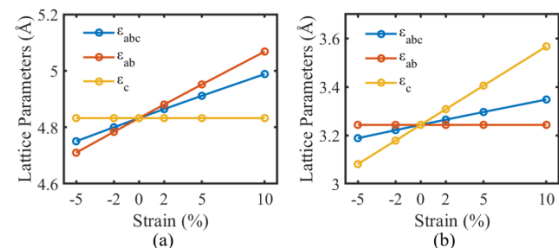


Figure 4. The effect of ϵ_{abc} , ϵ_{ab} , and ϵ_c strain to (a) a and b lattice parameters; (b) c lattice parameters in SnO_2 .

for the c lattice parameter. The given graphs show that the a , b , and c axis of ε_{abc} have a positive slope due to strain. Meanwhile, the effect of the ε_{ab} and ε_c strain shows constant behavior on the c -axis and ab -axis, respectively. The figures represent all the strain schemes in this paper.

The effect of each strain on the band structure evolution is shown in Figure 5(a) in PBEsol exchange-correlation and 5(b) in PBE0 form. Both figures depict the decreasing linear behavior in both PBEsol and PBE0 exchange-correlation parameters. Overall, the ε_{ab} and ε_c axis behave similarly to the triaxial computation, with the energy gap value decreasing as the lattice volume increases. The bandgap result calculation using PBE0 describes the semiconductor behavior on both positive and negative strains, where the positive strain reduces the energy gap, and the negative strain increases the bandgap. Then, the energy gap calculation using PBEsol shows semiconductor behavior; however, when the applied strain is more than 5%, the system shifts to conductor behavior due to the line passing through the Fermi energy and resulting in gapless between VBM and CBM.

This bandgap result is in good agreement with Kerrami *et al.* [5] and Zhou *et al.* [15] since the relationship between strain to the bandgap is strongly influenced by the covalent bonding interaction between Sn-O in the conduction band. The study that has been done before explained that the hybridization interaction in the conduction band becomes shorter when a compressive strain is employed [5]. The increase in the energy gap is defined by the fact that as more compressive strain is added to the system, the charge distribution at Sn sites will likewise grow due to the charge transfer from O to Sn. Under the tensile strain, the conduction band shifts down due to the sensitivity to strain. In contrast, the valence band remains almost constant, leading to the energy gap deduction.

Each strain axis direction has a bandgap slope, as shown in Figure 5, where the results are different from each other, thus indicating how easily the bandgap is manipulated by strain. A linear regression relationship in (2) can be used to calculate the slope between the bandgap and the strain.

$$E_{gap,PBE0}^{SnO_2} = \gamma\varepsilon + \chi \quad (2)$$

where γ is the slope, ε is the strain, and χ is the intercept.

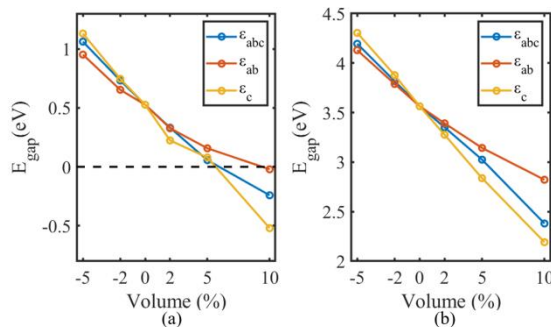


Figure 5. Effect of strain axis direction to bandgap evolution for (a) PBEsol; (b) PBE0 exchange-correlation for each strain scheme.

The slope and intercept calculation using (2) results are presented in Table 3. The uniaxial strain shows the highest slope value with -0.40 , followed by the triaxial and biaxial strains. The higher the slope value, the more reactive the system is to the strain changes. This study revealed that the largest or the smallest bandgap could be achieved by varying strain simply on the c -axis as the optimum manipulation of the SnO₂ structure.

Further explanation about the strain effects on the band structure is illustrated in Figure 6(a), (b), and (c) for ε_{abc} , ε_{ab} , and ε_c , respectively. The band structure was investigated in the range $M - \Gamma - Z$ magnitude, where the gap occurs between those directions. All the bandgap results for each strain variation show that the minimum bandgap is in the Γ direction and keep the same direct behavior. Overall, the calculation result describes that the effect of the strain does not change the shape of the valence and conduction bands, only slightly pushing the band downwards as the strain increases. The effect of the strain for more than 5% using PBEsol functional can be seen in each picture in Figure 6. The result shows that the CBM and the VBM for 5% applied strain still have a very narrow bandgap with 0.05 eV and nearly touch conductor behavior. Meanwhile, the 10% applied strain shows an overlapping CBM and VBM, indicating that the system shifts to conductor behavior. It can be concluded that PBE0 results are shown since the result gives a better prediction compared to PBEsol on energy structure.

TABLE 3
THE SLOPE AND INTERCEPT RESULT FOR EACH STRAIN SCHEME

Axis directions	Slope (γ)	Intercept (χ)
ε_{abc}	-0.34	4.56
ε_{ab}	-0.25	4.34
ε_c	-0.40	4.74

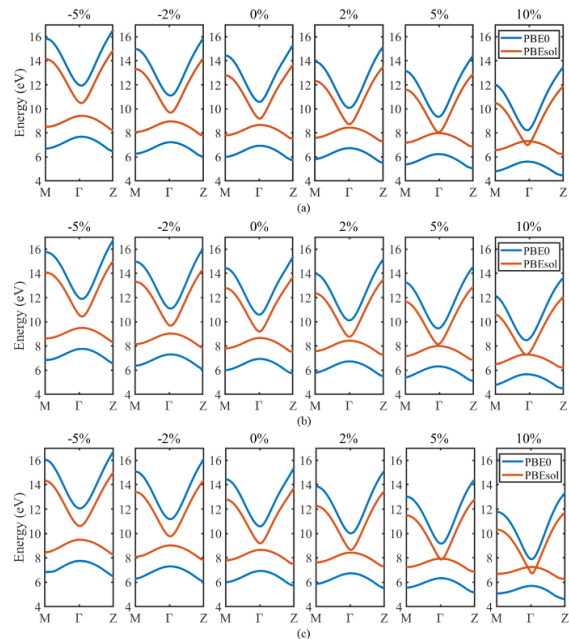


Figure 6. Bandgap structure of SnO₂ in three schemes strain employment: (a) ε_{abc} ; (b) ε_{ab} ; and (c) ε_c .

B. Thermoelectric Properties

The thermoelectric properties for all axis and strain variations of SnO₂ were calculated using both PBEsol and PBE0 functional in BOLTZWANN. The calculation results were then compared to the experimental values obtained by [5], [12], [29]. The Seebeck coefficient calculation results using PBEsol and PBE0 functional for several strain variations are depicted in Figure 7 at 100–800 K. Generally, the Seebeck coefficient value shows that SnO₂ under all strain variations has an *n*-type semiconductor. However, the Seebeck coefficient calculation using PBE0 functional has a striking difference compared to the PBEsol. The remarkable behavior occurs below 400 K, where all the Seebeck coefficients remain constant at $-3100 \mu\text{V/K}$, and then the line rises after 400 K, as shown in Figure 7(a) – (c). The strong correlation effect between *d*-orbital from tin atom and *p*-orbital from oxygen causes the experimental value is difficult to be replicated using both PBEsol and PBE0. Hence, the Seebeck coefficient behavior investigation continues with less accuracy. The comparison between the Seebeck coefficient obtained using PBEsol functional calculation and the experimental results that have been done before are shown in Figure 7(d). The data from Kartika *et al.* [12] were rescaled by 0.5 to fit in the graphic range because the magnitude is too great; however, this was done to make the explanation more understandable.

Overall, the Seebeck coefficient calculation has a similar pattern to all the experimental results where the Seebeck coefficient value reduced along with temperature increment. The Seebeck coefficient for the

compressive strain variations increased at a specific temperature. Meanwhile, the tensile strain variations decrease the Seebeck coefficient at the same temperature. This study identified the Seebeck coefficient result comparison between PBEsol and PBE0 calculation, describing that PBEsol gave a better prediction than PBE0 to the experimental value.

The electrical conductivity calculation of SnO₂ structure with tensile and compressive strains variations on triaxial directions is presented in Figure 8 for both PBEsol and PBE0 functional. Since the results for the uniaxial, biaxial, and triaxial directions exhibit comparable behavior, the triaxial strains were taken in order to compare the experimental results. In general, for both PBEsol and PBE0 calculation, the increasing temperature in the systems increases the electrical conductivity exponentially. However, the exact value for PBE0 is much lower than the PBEsol calculation result, about 10^{-8} :1 S/m magnitude. To ensure the validation of the calculation, the results are then compared with the electrical conductivity from the experimental result carried out by Paulson *et al.* [3]. The comparison is shown in Figure 8(a), where the experimental value is multiplied by 10^3 to make it easier to compare. From the presented figure, the behavior between the experimental value and PBEsol calculation shows similar tendencies rather than using the PBE0 calculation. Figure 8(b) describes a similar behavior with the Seebeck coefficient calculation with the PBE0 hybrid exchange parameter, where the electrical conductivity below 600 K remained constant and started to rise with a relatively small increment compared to PBEsol.

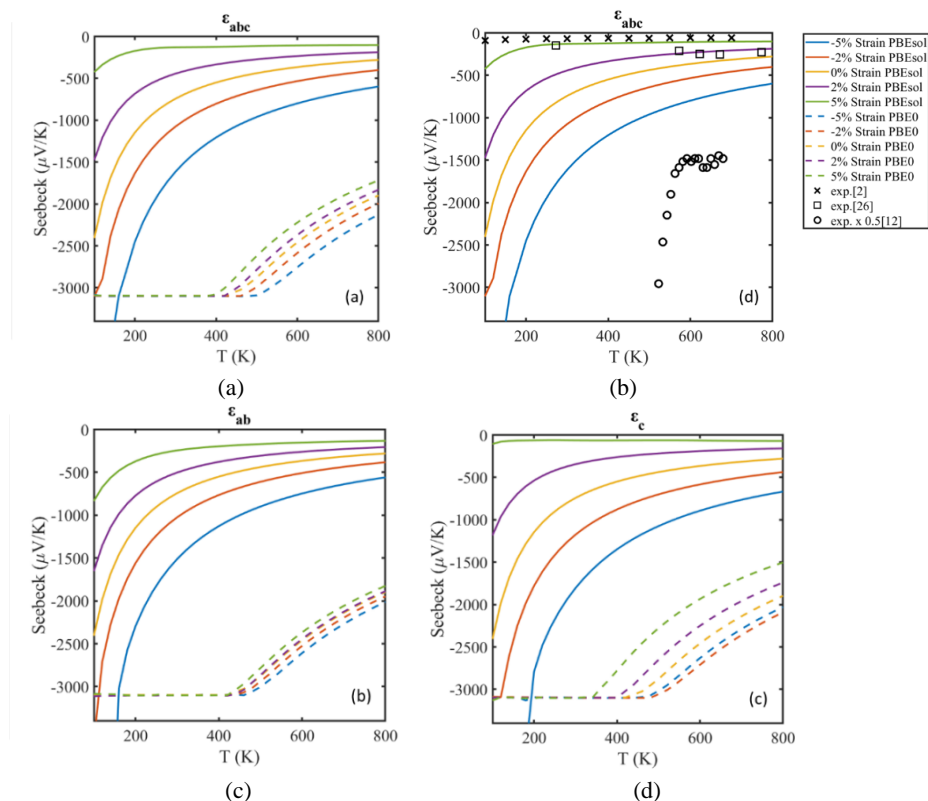


Figure 7. Seebeck coefficient calculation results for (a) triaxial axis; (b) comparison between the triaxial axis and experimental references value; (c). biaxial axis; (d) uniaxial axis.

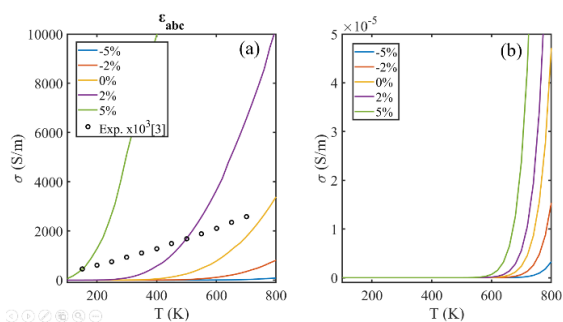


Figure 8. Electrical conductivity properties under compressive and tensile strains on triaxial directions were calculated using (a) PBEsol functional, and then compared with experimental references; (b) PBE0 functional.

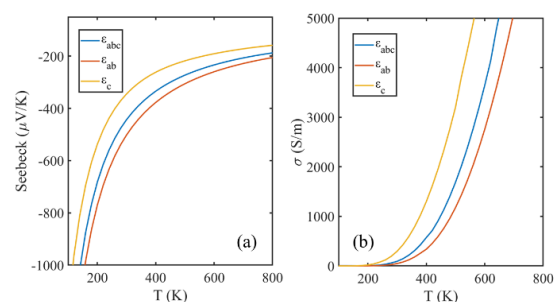


Figure 9. (a) Seebeck coefficient and (b) Electrical conductivity comparison value between triaxial, biaxial, and uniaxial with PBEsol exchange-correlation functional in 2% tensile strain.

In general, the tensile strain is more influential in enhancing electrical conductivity than the compressive strain. However, the results show the opposite when applied to the Seebeck coefficient calculation, where the tensile strain reduces the Seebeck value. The reduction of the Seebeck coefficient occurs due to the strongly correlated to the change of bandgap [30]-[31].

Further explanations about the tensile strain effect in this paper are summarized in Figure 9(a) for the Seebeck coefficient and 9(b) for the electrical conductivity calculation in +2% simulation. The figure depicts the order value from the highest to the lowest of the Seebeck coefficient and electrical conductivity for each scheme. The sequence of the Seebeck coefficient from the highest to the lowest is biaxial, triaxial, and uniaxial, whereas for electrical conductivity is the opposite, uniaxial, triaxial, then biaxial. This result also revealed that the simulation strategy could be determined from the desired result. For instance, to enhance the Seebeck coefficient, then the simulation can be done by manipulating the structure in the *ab*-axis direction, whereas using the structure in the *c*-axis during calculation will result in improved electrical conductivity.

IV. CONCLUSION

In conclusion, this paper studied the effect of compressive and tensile strains in uniaxial, biaxial, and triaxial directions on the electronic structure and thermoelectric properties using first-principal calculations. Comparison between PBEsol and PBE0 hybrid functional reveals that PBE0 gives the best estimation in SnO₂ bandgap structures. However, for thermoelectric properties prediction, PBEsol instead

gives the best performance. The strains engineering shows enhancement in the Seebeck coefficient for 2% and 5% compressive strain followed by a reduction in the electrical conductivity due to the change of the bandgap value. Strains application shows effectiveness when varying in uniaxial towards the *c*-axis since the results describe that the bandgap has more noticeable changes than other directions strain schemes. Furthermore, this study also highlighted that the strain manipulation could be deduced from the desired outcome. For example, changing structure in the *ab*-axis direction during simulation will increase the Seebeck coefficient, whereas using the structure in the *c*-axis during calculation will result in improved electrical conductivity.

DECLARATIONS

Conflict of Interest

The authors have declared that no competing interests exist.

CRediT Authorship Contribution

All authors are main contributors to this paper: Budi Adiperdana: Conceptualization, Software, Investigation, Methodology, Visualization, Writing - Original Draft; Nadya Larasati Kartika: Conceptualization, Methodology, Writing - Review & Editing; Irwan Ary Dharmawan: Resources, Supervision.

Funding

The authors received no financial support for the research, authorship, and/or publication of this article.

Acknowledgment

This study has been supported by Department of Geophysics Universitas Padjadjaran (RockExplorer) for the High Performance Computing facilities and Research Center for Advanced Materials BRIN.

REFERENCES

- [1] S. Das and V. Jayaraman, "SnO₂: a comprehensive review on structures and gas sensors," *Prog. Mater. Sci.*, vol. 66, pp. 112–255, Oct. 2014. doi: 10.1016/j.pmatsci.2014.06.003.
- [2] M. B. Sahana, C. Sudakar, A. Dixit, J. S. Thakur, R. Naik, and V. M. Naik, "Quantum confinement effects and bandgap engineering of SnO₂ nanocrystals in a MgO matrix," *Acta Mater*, vol. 60, no. 3, pp. 1072–1078, Feb. 2012, doi: 10.1016/j.actamat.2011.11.012.
- [3] A. Paulson, M. Sabeer, and P. P. Prayudmnan, "Enhanced thermoelectric property of oxygen deficient nickel doped SnO₂ for high temperature application," *Mater. Res. Express*, vol. 5, pp. 1–21, Apr. 2018, doi: 10.1088/2053-1591/aabd64.
- [4] S. Yu, L. Li, D. Xu, H. Dong, and Y. Jin, "Characterization of SnO₂/Cu/SnO₂ multilayers for high performance transparent conducting electrodes," *Thin Solid Films*, vol. 562, pp. 501–505, Jul. 2014, doi: 10.1016/j.tsf.2014.04.064.
- [5] Z. Kerrami, A. Sibari, O. Mounkachi, A. Benyoussef, and M. Benaissa, "SnO₂ improved thermoelectric properties under compressive strain," *Comput. Condens. Matter*, vol. 18, Mar. 2019, Art. no. e00356, doi: 10.1016/j.cocom.2018.e00356.
- [6] A. J. Minnich, M. S. Dresselhaus, Z. F. Ren, and G. Chen, "Bulk nanostructured thermoelectric materials: current research and future prospects," *Energy Environ. Sci.*, vol. 2, no. 5, pp. 466–479, Feb. 2009, doi: 10.1039/b822664b.
- [7] G. S. Nolas, J. Sharp, and J. Goldsmid, *Thermoelectrics: basic principles and new materials developments*, 1st ed., Heidelberg, Germany: Springer Berlin, 2013, doi: 10.1007/978-3-662-04569-5.

- [8] A. R. Nugraha, N. L. Kartika, Dedi, and A. A. Nugroho, "Thermoelectric properties of SnO₂/Bi₂Te₃ composite," *Mater. Sci. Forum*, vol. 1028, pp. 99–104, Apr. 2021, doi: 10.4028/www.scientific.net/MSF.1028.99.
- [9] S. Fayette, D. S. Smith, A. Smith, and C. Martin, "Influence of grain size on the thermal conductivity of tin oxide ceramics," *J. Eur. Ceram. Soc.*, vol. 20, no. 3, pp. 297–302, Mar. 2000, doi: 10.1016/S0955-2219(99)00171-5.
- [10] M. M. Bagheri-Mohagheghi, N. Shahtahmasebi, M. R. Alinejad, A. Youssefi, and M. Shokoh-Saremxi, "Fe-doped SnO₂ transparent semi-conducting thin films deposited by spray pyrolysis technique: thermoelectric and p-type conductivity properties," *Solid State Sci.*, vol. 11, no. 1, pp. 233–239, Jan. 2009, doi: 10.1016/j.solidstatesciences.2008.05.005.
- [11] K. Rubenis, S. Populoh, P. Thiel, S. Yoon, U. Müller, and J. Locs, "Thermoelectric properties of dense Sb-doped SnO₂ ceramics," *J. Alloys Compd.*, vol. 692, pp. 515–521, Jan. 2017, doi: 10.1016/j.jallcom.2016.09.062.
- [12] N. L. Kartika *et al.*, "Thermopower enhancement of rutile-type SnO₂ nanocrystalline using facile co-precipitation method," *J. Elektr. Telekom.*, vol. 20, no. 2, pp. 82–88, Dec. 2020, doi: 10.14203/jet.v20.82-88.
- [13] F. Delorme *et al.*, "Nanostructuring of dense SnO₂ ceramics by spark plasma sintering," *Ceram. Int.*, vol. 45, no. 7, pp. 8313–8318, May 2019, doi: 10.1016/j.ceramint.2019.01.138.
- [14] N. Kumar, G. K. Sidhu, and R. Kumar, "Correlation of synthesis parameters to the phase segregation and lattice strain in tungsten oxide nanoparticles," *Mater. Res. Express*, vol. 6, no. 7, Apr. 2019, Art. no. 0750 doi: 10.1088/2053-1591/ab12a5.
- [15] W. Zhou, Y. Liu, Y. Yang, and P. Wu, "Bandgap engineering of SnO₂ by epitaxial strain: experimental and theoretical investigations," *J. Phys. Chem. C.*, vol. 118, no. 12, pp. 6448–6453, Mar. 2014, doi: 10.1021/jp500546r.
- [16] H. Absike, M. Hajji, H. Labrim, B. Hartiti, and H. Ez-Zahraouy, "Strain effects on the electronic and thermoelectric properties of copper oxide," *Comput. Condens. Matter*, vol. 16, Sep. 2018, Art. no. e00322 doi: 10.1016/j.cocom.2018.e00322.
- [17] W. Kohn and L. J. Sham, "Self-consistent equations including exchange and correlation effects," *Phys. Rev.*, Nov. 1965, Art. no. A1133, doi: 10.1103/PhysRev.140.A1133.
- [18] J. P. Perdew *et al.*, "Restoring the density-gradient expansion for exchange in solids and surfaces," *Phys. Rev. Lett.*, vol. 100, no. 13, Apr. 2008, Art. no. 136406, doi: 10.1103/PhysRevLett.100.136406.
- [19] J. W. Song, K. Yamashita, and K. Hirao, "Communication: a new hybrid exchange correlation functional for bandgap calculations using a short-range Gaussian attenuation (Gaussian-Perdew-Burke-Ernzerhof)," *J. Chem. Phys.*, vol. 135, no. 7, Aug. 2011, Art. no. 071103, doi: 10.1063/1.3628522.
- [20] C. Adamo and V. Barone, "Toward reliable density functional methods without adjustable parameters: the PBE0 model," *J. Chem. Phys.*, vol. 110, no. 13, pp. 6158–6170, Mar. 1999, doi: 10.1063/1.478522.
- [21] J. Heyd, G. E. Scuseria, and M. Ernzerhof, "Hybrid functionals based on a screened coulomb potential," *J. Chem. Phys.*, vol. 118, no. 18, pp. 8207–8215, May 2003, doi: 10.1063/1.1564060.
- [22] P. Giannozzi *et al.*, "Quantum espresso: a modular and open-source software project for quantum simulations of materials," *J. Phys. Condens. Matter*, vol. 21, no. 39, Jun. 2009, Art. no. 395502, doi: 10.1088/0953-8984/21/39/395502.
- [23] P. E. Blöchl, "Projector augmented-wave method," *Phys. Rev. B*, vol. 50, no. 24, pp. 17953–17979, Dec. 1994, doi: 10.1103/PhysRevB.50.17953.
- [24] A. A. Mostofi *et al.*, "An updated version of Wannier90: a tool for obtaining maximally-localized Wannier functions," *Comput. Phys. Commun.*, vol. 185, no. 8, pp. 2309–2310, Aug. 2014, doi: 10.1016/j.cpc.2014.05.003.
- [25] G. Pizzi, D. Volja, B. Kozinsky, M. Fornari, and N. Marzari, "BoltzWann: a code for the evaluation of thermoelectric and electronic transport properties with a maximally-localized Wannier functions basis," *Comput. Phys. Commun.*, vol. 185, pp. 422–429, May 2013, doi: 10.1016/j.cpc.2013.09.015.
- [26] K. B. Spooner, A. M. Ganose, and D. O. Scanlon, "Assessing the limitations of transparent conducting oxides as thermoelectrics," *J. Mater. Chem. A*, vol. 8, no. 24, pp. 11948–11957, Jun. 2020, doi: 10.1039/d0ta02247k.
- [27] D. O. Scanlon and G. W. Watson, "On the possibility of p-type SnO₂," *J. Mater. Chem.*, vol. 22, no. 48, pp. 25236–25245, Dec. 2012, doi: 10.1039/c2jm34352e.
- [28] P. Ágoston, K. Albe, R. M. Nieminen, and M. J. Puska, "Intrinsic n-type behavior in transparent conducting oxides: a comparative hybrid-functional study of In₂O₃, SnO₂, and ZnO," *Phys. Rev. Lett.*, vol. 103, no. 24, Dec. 2009, doi: 10.1103/PhysRevLett.103.245501.
- [29] M. Ferreira, J. Loureiro, A. Nogueira, A. Rodrigues, R. Martins, and I. Ferreira, "SnO₂ thin film oxides produced by rf sputtering for transparent thermoelectric devices," *Mater. Today Proc.*, vol. 2, no. 2, pp. 647–653, 2015, doi: 10.1016/j.matpr.2015.05.090.
- [30] Q. Wang, L. Han, L. Wu, T. Zhang, S. Li, and P. Lu, "Strain effect on thermoelectric performance of in-se monolayer," *Nanoscale Res. Lett.*, vol. 14, no. 1, Dec. 2019, doi: 10.1186/s11671-019-3113-9.
- [31] H. J. Goldsmid and J. W. Sharp, "Estimation of the thermal bandgap of a semiconductor from seebeck measurements," *J. Electron. Mater.*, vol. 28, pp. 869–872, Jul. 1999, doi: 10.1007/s11664-999-0211-y.